Ultrasound assisted dispersal of a copper nanopowder for electroless copper activation

Graves, J. , Sugden, M. , Litchfield, R.E. , Hutt, D.A. , Mason, T.J. and Cobley, A.

Original citation & hyperlink:
Graves, J. , Sugden, M. , Litchfield, R.E. , Hutt, D.A. , Mason, T.J. and Cobley, A. (2015) Ultrasound assisted dispersal of a copper nanopowder for electroless copper activation. Ultrasonics Sonochemistry, volume 29 : 428-438
http://dx.doi.org/10.1016/j.ultsonch.2015.10.016

DOI 10.1016/j.ultsonch.2015.10.016
ISSN 1350-4177
ESSN 1873-2828

Publisher: Elsevier

Ultrasound Assisted Dispersal of a Copper Nanopowder for Electroless Copper Activation

John E. Graves, Mark Sugden, Robert E. Litchfield, David A. Hutt, Timothy J. Mason, Andrew J. Cobley

PII: S1350-4177(15)30059-6
DOI: http://dx.doi.org/10.1016/j.ultsonch.2015.10.016
Reference: ULTSON 3021

To appear in: *Ultrasonics Sonochemistry*

Received Date: 3 December 2014
Revised Date: 15 October 2015
Accepted Date: 23 October 2015

Please cite this article as: J.E. Graves, M. Sugden, R.E. Litchfield, D.A. Hutt, T.J. Mason, A.J. Cobley, Ultrasound Assisted Dispersal of a Copper Nanopowder for Electroless Copper Activation, *Ultrasonics Sonochemistry* (2015), doi: http://dx.doi.org/10.1016/j.ultsonch.2015.10.016

Ultrasound Assisted Dispersal of a Copper Nanopowder for Electroless Copper Activation.

John E. Graves[a*], Mark Sugden[b], Robert E. Litchfield[b], David A. Hutt[b], Timothy J. Mason[c] , Andrew J. Cobley[a]

[a] Functional Materials Applied Research Group, Coventry University, Priory Street, Coventry, CV1 5FB, UK
[b]Wolfson School of Mechanical and Manufacturing Engineering, Loughborough University, Loughborough, Leicestershire LE11 3TU, UK
[c]The Sonochemistry Centre at Coventry University, Faculty of Health and Life Sciences, Priory Street, Coventry CV1 5FB, UK

* Corresponding author. Tel: +442477 658624. E-mail address: j.graves@coventry.ac.uk

Abstract

This paper describes the ultrasound assisted dispersal of a low wt. / vol. % copper nanopowder mixture and determines the optimum conditions for de-agglomeration. A commercially available powder was added to propan-2-ol and dispersed using a magnetic stirrer, a high frequency 850 kHz ultrasonic cell, a standard 40 kHz bath and a 20 kHz ultrasonic probe. The particle size of the powder was characterized using dynamic light scattering (DLS). Z-average diameters (mean cluster size based on the intensity of scattered light) and intensity, volume and number size distributions were monitored as a function of time and energy input. Low frequency ultrasound was found to be more effective than high frequency ultrasound at de-agglomerating the powder and dispersion with a 20 kHz ultrasonic probe was found to be very effective at breaking apart large agglomerates containing weakly bound clusters of nanoparticles. In general, the breakage of nanoclusters was found to be a factor of ultrasonic intensity, the higher the intensity the greater the de-agglomeration and typically micron sized clusters were reduced to sub 100nm particles in less than 30 min using optimum conditions. However, there came a point at which the forces generated by ultrasonic cavitation were either insufficient to overcome the cohesive bonds between smaller aggregates or at very high intensities decoupling between the tip and solution occurred. Absorption spectroscopy indicated a copper core structure with a thin oxide shell and the catalytic performance of this dispersion was demonstrated by drop coating onto substrates and subsequent electroless copper metallization. This relatively inexpensive catalytic suspension has the potential to replace precious metal based colloids used in electronics manufacturing.

Keywords

Ultrasound
Dispersion
Copper Nanoparticles
Catalytic Ink
Electroless Copper

1. Introduction

Electroless copper plating is a widely used industrial process in the electronics manufacturing industry for the metallization of non-conducting substrates such as polymers, glass and ceramics [1-2]. For such plating, commercially available precious metal based tin-palladium [3] catalysts are typically used. Because of its scarcity the high and fluctuating cost of palladium makes the process expensive, and there have been numerous attempts to develop viable catalysts based on less noble metals [4-7]. A potential catalyst material that can be used to activate the surface is copper in the form of a nanopowder [8]. However, they are supplied in the form of dry powders and have to be re-dispersed in a liquid phase to give homogenous stable solutions comprising of clusters that need to be broken into primary nanoparticles during the dispersion process. Dispersion and de-agglomeration of nanopowders in liquids can be carried out in ball mills [9], rotor-stator high shear mixers [10] or ultrasonic processors. Ultrasonic dispersion is a very effective technique for dispersing a powder in a liquid [11]. The dispersion mechanism involves acoustic cavitation (through the formation, growth and implosion of bubbles resulting in the rupture of agglomerates) and acoustic streaming. One of the first papers published using this technique investigated the effects of high intensity ultrasound on micron-sized inorganic solids with powders of 60 - 90 µm diameter being reduced to 5-10 µm in diameter after a few minutes of ultrasonic irradiation [12]. A number of nanomaterials that have been the subject of recent dispersion investigations include goethite [13,14] , silica [15-19] , haematite

[20], barium titanate [21], zinc oxide [22], carbon black [23], silver [23], alumina [24-26] and carbon nanotubes [27]. In many of these studies, high intensity ultrasonic processing was found to de-agglomerate and decrease the size of the starting materials. The intense forces generated by cavitation are large enough to exceed the cohesive bonds between particles and fragment agglomerates into smaller aggregates and primary particles. For graphite, forces resulting from cavitation have been used to cleave layers to form graphene [28,29]. However, de-agglomeration efficiency depends upon many factors and each individual material needs to be studied in turn.

Despite the numerous publications on ultrasonic dispersion of nanoparticles in liquid media, to the best of our knowledge only two specific studies have focused on the effects of ultrasound on copper powders [30,31]. Suslick et al. studied micron sized powders and concluded that 20 kHz ultrasonic irradiation enhances the reactivity of the powder and that these effects are due to interparticle collisions and the removal of surface oxides. In a previous paper we have demonstrated the potential for ultrasonic de-agglomeration of copper nanoparticles using a 40 kHz ultrasonic bath and its use as an activator for electroless copper plating [8]. In this paper we have expanded the study and report for the first time on the dispersion of a low concentration mixture of copper nanoparticles in propan-2-ol (0.1g dm^{-3}) using three different ultrasonic frequencies (20 kHz, 40 kHz and 850 kHz) at different times and powers. The degree of de–agglomeration / dispersal was measured and the catalytic behaviour of the copper powder as an inexpensive ink for electroless copper plating was assessed.

2. Materials and Methods

2.1 Materials

Commercial copper nanoparticles (Cu, 99.8%, primary particle size 25nm) were supplied in dry powder form in sealed pouches. The pouches were opened in a nitrogen purged glove box or glove bag and stored under nitrogen. Propanol-2-ol (HPLC grade) was purchased from Fisher Scientific and filtered through a 0.20 µm GNWP nylon membrane before use. Chemically synthesised copper nanoparticles were also prepared using the procedure described by Grouchko et al. [32].The tin/ palladium colloidal catalyst (Catalyst 3344, 0.015 wt./ vol.% Pd) and electroless copper chemistries (Circuposit 3350-1) were supplied by Chestech Ltd and prepared according to the product data sheets. The electroless copper bath was operated at the top end of the recommended temperature range, 52°C. FR-4 substrate (Isola 370HR), a typical printed circuit board laminate, was supplied by Graphic plc.

2.2 Equipment

A Sonic and Materials Inc. probe, Model VC 750, was used for generating 20 kHz ultrasound with a maximum power output of 750 W. The high-frequency voltage output of the generator was transferred into mechanical vibrations by piezoelectric transducers in an exponential horn with a tip diameter of 1.3 cm. For higher ultrasonic intensity tests a tapered micro-tip (Sonic and Materials, Part No. 630-0420) with a diameter of 0.6 cm was also used. Experiments at 40 kHz were carried out using a single transducer ultrasonic bath (Langford Sonomatic), Model 375TT, power output 75 W, 2.3

litre volume. The bath was filled with 2 litres of water and 1 % v/v Decon solution and the beaker positioned in the centre of the bath. The bottom of the beaker was fixed at 4.5 cm from the transducer. The mixture was stirred using a four blade propeller head stirrer (Fisher Scientific, Product code 11829694) powered by an overhead unit (Stuart Scientific), Model SS-10 at 250 rpm. A 850 kHz, 100 W, single transducer (4 cm diameter), ultrasonic generator, (Meinhardt, Type K80-5) operating at level intensity 4 with continuous pulse setting, was used for the high frequency work and an overhead stirrer was also used to agitate the mixture, as above.

The ultrasonic baths and probes were calibrated using the calorimetry method [11] with propan-2-ol. Recorded ultrasonic energy densities for the 40 kHz and 850 kHz bath were 0.13 W cm^{-3}. For the 20 kHz probe with the 1.3 cm diameter replaceable tip ultrasonic energy densities of 0.13, 0.33, 0.47, 0.72 and 0.99 W cm^{-3} were recorded at 20, 40, 60, 80 and 100% amplitude and for the 20 kHz probe fitted with a 0.6 cm tapered tip ultrasonic energy densities of 0.22 and 0.34 W cm^{-3} were recorded at 40 % and 60 % amplitudes respectively. In addition, in order to compare the two 20 kHz ultrasonic horn configurations, power intensities were calculated by dividing the ultrasonic power entering the system by the area of the probe tip. For the amplitudes listed above, intensities of 10, 25, 35, 55 and 75 W cm^{-2} and 75 and 120 W cm^{-2} were calculated for the 1.3 cm and 0.6 cm tips respectively.

The morphology of the copper nanopowder was characterized by field emission scanning electron microscopy (LEO 1530 VP Field Emission SEM) and scanning transmission electron microscopy (A JEOL 2000FX STEM). Samples for SEM were prepared by dusting the powder onto adhesive carbon

supports stuck onto aluminium SEM stubs. The samples were then sputter coated with gold/palladium for 60 seconds. STEM samples were prepared by dispersing the powder in propan-2-ol and then pipetting one drop onto a holey carbon film on a 200 or 300 mesh copper grid placed on top of filter paper. The filter paper absorbed any excess alcohol. The grid was dried and then placed in the STEM for examination.

Samples of dispersions were also studied by absorption spectroscopy from a double beam spectrophotometer (Shimadzu UV-1800 Spectrophotometer) in the wavelength range 400-800 nm.

2.3 Dispersion

A typical procedure used to prepare the dispersions was: 10 mg of copper nanopowder and 100 cm^3 of propan-2-ol were placed in a 150 cm^3 tall form glass beaker to give a 0.01 wt. / vol. % mixture. For the 20 kHz bath the probe tip was immersed 4 cm into the solution. Continuous ultrasonic irradiation was applied to the mixture and the processing sample was cooled using an ice-water bath that kept the temperature of the dispersions between 35 and 55°C. At certain time intervals a sample was removed from the beaker, placed in a glass cuvette and analysed using dynamic light scattering (DLS) with a Zetasizer S (Malvern Instruments Ltd, Malvern, UK). Intensity – size distribution graphs, Z-average (mean cluster size based on the intensity of scattered light) and polydispersity index values were recorded. Each measurement was typically 12 individual measurements of at least 10 s in length and each distribution / Z-average diameter presented here was an

average of three consecutive measurements taken automatically at 2-3 minute intervals.

3. Results and Discussion

3.1. Copper nanoparticle characterization

A SEM image of the as received dry copper nanopowder is shown in Figure 1. The particles are almost spherical and there are larger clusters present which are agglomerates of the primary particle size. The SEM image shows a mottled effect on the surface of the particles which is probably an artefact of the sample preparation. The image also suggests the primary particle size is between 25 -100 nm. TEM images of the as received powder dispersed with a very short 10 s pulse of ultrasound are shown in Figure 2. The nanoparticle clusters are typically between 0.5 – 1.0 μm in one dimension before extensive processing, Figure 2 (a) and show a typical cluster / agglomerate structure which is susceptible to breakdown under sonication, Figure 2 (b).

3.2 Ultrasonic dispersion in propan-2-ol.

Propan-2-ol was chosen as a suitable dispersing solvent for two reasons; (a) it dissolves a wide range of non-polar compounds and is therefore a good solvent for dissolving potential organic capping agents for subsequent coating of the copper nanoparticles and (b) it is miscible with water, relatively non-toxic and is known to be used as a solvent for ink-jet inks.

3.2.1 Effect of ultrasonic frequency.

Production and intensity of cavitation is affected by ultrasonic frequency; in qualitative terms bubble sizes and cavitation forces differ according to the applied frequency. To investigate the effect of ultrasonic frequency on de-agglomeration mixtures of copper nanopowder in propan-2-ol were subjected to three different ultrasonic frequencies; 20, 40 and 850 kHz. In order to make the comparison between different types of ultrasonic equipment an energy density of 0.13 W cm^{-3} was used for the 40 kHz ultrasonic bath (fixed power), the 20 kHz ultrasonic probe (20 % amplitude) and the 850 kHz system. Figure 3 displays a plot of the Z-average of the copper nanoparticle clusters dispersed in 100 cm^3 solvent, for each operating frequency as a function of time. It can be seen that the Z-average for the sample subjected to 850 kHz high frequency ultrasound shows very little change in the mean cluster size with time. At 40 kHz and 20 kHz the decrease in the observed Z- average value is more pronounced but slows with increasing time. These observations of the difference between high and low frequencies can be explained in terms of the much shorter acoustic cycle and smaller bubble size at the higher frequency. Smaller bubbles have a less violent cavitation collapse leading to lower fluid velocities and shear forces. At low frequency, where a long acoustic cycle exists, large bubbles are created; collapse is more violent leading to more extreme conditions which aid particle de-agglomeration [33,34].

3.2.2. 20 kHz replaceable tip and tapered tip ultrasonic processing

With improved de-agglomeration observed using low frequency ultrasound, investigations focused on the use of a 20 kHz ultrasonic probe

where it was possible to vary the transducer energy and thus the energy transmitted to the solution. Vibration amplitudes of 20%, 40%, 60%, 80% and 100% were applied to a 1.3 cm diameter replaceable tip corresponding to power intensities of 10, 25, 35, 55 and 75 W cm^{-2}. (Power intensity has been quoted for the horn system because it is a more realistic measure of the acoustic intensity near to the tip of the probe. The power is delivered to a much smaller area directly into the dispersion in comparison to bath systems.) Figure 4 shows the plot of the mean copper nanoparticle cluster size for different operating intensities (a) as a function of ultrasonic processing time and (b) as a function of specific energy input. For the lower powers (≤ 40% amplitude) a low breakage rate of the nanopowder clusters is observed and final cluster sizes are greater (175+ nm). Higher powers lead to greater breakage rates and the lowest recorded Z-average values (135 nm at 100% amplitude after 150 min processing time). Clearly, the higher the operating amplitude / intensity the greater the reduction in the size of the copper nanopowder clusters. Furthermore, the plots of Z-average as a function of time show power law dependence in that the majority of the de-agglomeration or breakage occurs over the first 45 minutes of ultrasonic processing. Evidence for this is provided in Table 1 which records the % reduction in Z-average values between 15 - 45 min and 90 - 120 minutes for the intensities investigated. The major reduction ranging from 8 – 12 % occurred between 15 - 45 minutes and only a further 2-4 % resulted from prolonged sonication for 90-120 minutes. From this it seems reasonable to conclude that the use of extended processing times is not warranted. Figure 4 (b) records the Z-average as a function of specific energy input into the system (in terms of kJ /

cm^3) and confirms that for 20 kHz processing the intensity generated at the tip of the horn is more critical than the total energy input into the system for de-agglomeration of the powder. High horn intensities are known to increase the intensity of bubble collapse and consequently the concentration of resulting forces produced in a “cone” of high energy emanating from the end of an ultrasonic horn leads to smaller copper nanoparticle cluster sizes. These features of ultrasonic processing are in agreement with studies of other powders reported in the literature [18,19,22].

SEM and TEM evidence suggests the primary particle size of the copper nanopowder varies between 25 – 100 nm. The Z-average values recorded above did not approach this value. However there is some evidence to suggest that processing at higher ultrasonic amplitudes does lead to the formation of sub 100 nm cluster populations. Typical size distribution-intensity plots for an amplitude of 100%, over a range of ultrasonic processing times, are shown in Figure 5. Particle size distributions before the application of ultrasound are difficult to measure because of the interference of micron sized particles which scatter significantly more light than nanoparticles. Nevertheless curve (a) does illustrate a typical result when the copper nanopowder is dispersed for one hour at 500 rpm using a magnetic follower. A tri-modal distribution is observed with peaks at 120, 710, and 5500 nm. Curves (b-f) show size distribution curves after 1, 15, 30, 60 and 90 min of 20 kHz ultrasonic processing respectively. After one minute of processing the rapid fragmentation of large agglomerates has occurred and the dispersion is mono-modal, with a peak intensity of 225 nm. The peak is shifted to the left

after 15 – 30 min of processing to 190 nm and indicates large agglomerates are being broken down into smaller components. After 60 min of processing the peak is again shifted to the left to 165 nm and with 90 min of processing the peak remains centred around 165 nm, but the intensity has increased and the peak distribution narrows. This is confirmed by a decrease in the polydispersity index from 0.22 to 0.17 indicating an improved mono-modal dispersion. Figure 6 shows size distributions as a function of volume (a) and as a function of number (b) recorded from a sample processed at 100% amplitude, 20 kHz for 15, 30 and 60 minutes. Two peaks between 30 - 40 nm and 255 nm are observed in the volume distribution plot and although large errors can occur in generating number distribution plots from intensity data, graph (c) does provide evidence that two populations of sub 100 nm particles are present in the sample with peak populations between 30 – 40 nm and 60 - 70 nm.

In order to increase the vibrational amplitude of the horn system the 1.3 cm end diameter cylindrical horn as used above was changed to a tapered horn with a smaller end diameter. Because the end diameter of the horn is smaller than the area attached to the driving transducer element there will be a magnification of the ultrasonic vibration (i.e. power) [11]. A tapered horn of end diameter 0.6 cm was used and Figure 7(a) records a plot of Z-average as a function of ultrasonic time for this system operating at amplitudes of 40% and 60 % and compares the results with those obtained using the 1.3 cm probe operating at amplitudes of 40 % and 100 %. The ultrasonic intensities at these settings were 75 and 120 W cm^{-2} and 25 and 75 W cm^{-2} respectively. Again the curves demonstrate power law dependence where most of the

breakage occurs during the first 45 minutes of processing. It would appear at first sight that the results obtained for the tapered tip are not as good as those obtained from the 1.3 cm tip. However, when the Z-average is plotted as a function of specific energy input (Figure 7b) the trend lines for intensities of 75 W cm^{-2} collapse onto each other and the de-agglomeration performance is matched. At very high intensities of 120 W cm^{-2} there is no significant increase in the breakage rate or decrease in the copper nanopowder cluster size; the result is the same as that for an intensity of 75 W cm^{-2}. This can be ascribed to the decoupling effect where the amplitude of vibration becomes too large to maintain continuous contact between the emitting surface and the liquid causing a reduction in the effective power entering the system. It may also be the result of the surface forces between the particles being stronger than the hydrodynamic forces created by ultrasonic cavitation so that the particles cannot be broken down any further by mechanical action alone.

3.3. TEM and absorption spectroscopy of dispersed copper nanoparticles

TEM images after ultrasonic processing are shown in Figure 8 (a) – (d). Typically, sub 50 nm particles are present in the samples, see 8(a) and (c), along with larger clusters, (b) and (c), which have broken off agglomerates after sonication, see Figure 2. These findings support the DLS results that indicate the presence of sub 100 nm particles. There is also evidence to suggest large aggregates are still present after ultrasonic processing. Figure 8 (d) shows a low magnification image with a cluster of large aggregates located by the edge of a hole in the TEM grid with smaller particles in the background. The presence of a few of these larger clusters, which show a

reluctance to be broken down by the forces generated by ultrasound, probably account for Z-average values staying above 135+ nm. It is unclear why some agglomerates remain as large aggregates. It may be due to some inconsistencies in the way the nanoparticles are synthesised; particles become fused together and form strong bonds during the manufacturing process or more likely sintering of the pure copper nanopowder occurs during storage in vacuum sealed pouches. This would also account for the extended ultrasonic processing times required to disperse these particles when typically only a few seconds or a few minutes are required to disperse other types of powders.

Further evidence for nanoparticle structure was obtained by recording absorption spectra from dispersed samples. Figure 9 presents the absorption spectra from a chemically synthesised copper nanoparticle sample, Z-average 46 nm (a), a dispersed copper nanopowder after 20 kHz ultrasonic processing (b) and the dispersed copper nanopowder after the addition of glacial acetic acid, 4% by vol. (c) – (k). The dispersion of chemically synthesised copper nanoparticles is characterized by a red wine colour and has a characteristic absorption peak at ~ 560 nm due to the plasmon effect [32]. The dispersions of copper nanopowders prepared using an ultrasonic horn are black in colour, see Figure 10 before (a) and after dispersion (b), and have an absorption peak at ~ 618 nm. The shift to the higher wavelength for the surface plasmon resonance (SPR) can be attributed to the morphology or symmetry of the copper nanostructures [35,36]. Spectra (c) – (k) show the response after the addition of glacial acetic acid to the dispersion. Glacial acetic acid dissolves copper oxides and copper at a slow rate allowing enough time for absorption

spectra to be recorded on a standard spectrophotometer. A slight initial blue shift of the absorbance maximum was observed from 618 nm to 610 nm after 1 min, but no significant shift was noted. It is known that the SPR of copper nanoparticles is significantly affected by the presence of copper oxides leading to a shift in the SPR to a wavelength between 700 – 800 nm [37]. Therefore an initial absorption peak at 618nm suggests the nanoparticles are relatively oxide free and this observation is supported by the fact that a similar spectrum is recorded after the addition of glacial acetic acid. Increasing time reduces the SPR until the glacial acetic acid dissolves the copper nanoparticles and it disappears.

The results from DLS, TEM and absorption spectroscopy confirm that the breakage behaviour of the copper nanopowder is consistent with an erosion mechanism. The agglomerates are gradually reduced in size by the breakage of fine particles (sub 100 nm) from their surface. A point is reached where no significant fragmentation takes place and the rate of change in size decreases. These observations are consistent with previous studies reported in the literature for silica, titania [18,19], and zinc oxide powders [22]. Occasionally, re-agglomeration of the dispersed copper nanopowder was observed at high operating amplitudes and longer processing times. Previous work has also reported this observation [24]. However, this process could not be predicted or reproduced consistently.

It is worth noting that throughout this study there was no evidence to suggest that primary particles can be broken into smaller nanoparticles. This finding also agrees with previous work in this area where it was found that

agglomerates held together by weak material bridges or weak forces can be broken down into primary components, but aggregates created by covalent bonds cannot be separated into smaller clusters [16,24].

3.4. Electroless Copper Activation

The deposition of a thin metallic copper layer onto a non-conductive substrate by electroless plating requires the previous formation of catalytic sites on the surface. The catalyst particles need to have an active surface for formaldehyde oxidation which releases electrons and subsequently reduces copper(II) ions in solution to the metallic state on the object to be coated. The most prevalent system in commercial use is a tin – palladium colloid. The continued use of palladium is problematic in terms of its expense and scarcity and an alternative non-precious metal catalyst is desirable.

A copper nanoparticle / propan-2-ol mixture (0.01 wt. / vol. %), dispersed with a 20 kHz ultrasonic probe (1.3 cm diameter tip, 100% amplitude), was evaluated as an activator for electroless copper plating by drop coating a fixed volume (0.5 cm^3), onto an FR-4 substrate. FR-4 is the primary insulating material upon which the vast majority of rigid printed circuit boards are produced. Samples were removed from the dispersion at various stages of de-agglomeration, dropped onto the FR-4 surface and then dried on a hot plate before being placed into an electroless copper bath. Figure 11 displays SEM micrographs obtained from FR-4 substrates as received (a) and after electroless copper plating for 25 mins following activation by drop coating with copper nanoparticle dispersions prepared with 1 min (b) 15 min (c) and 30 min (d) of ultrasonic processing. For comparison a sample dip

coated in a Sn / Pd colloidal catalyst, rinsed and metallized in electroless copper is also shown (e). Micrographs (b) – (d), show that the dispersed copper nanopowder has adsorbed onto the substrate to form catalytic islands, initiated electroless copper plating and subsequently grown in size. However, different degrees of substrate coverage are observed. Large areas of FR-4 can be seen in between plated clusters in (b), micrograph (c) shows areas where the copper islands have started to overlap and cover more of the substrate and in (d) the copper islands have overlapped to form an almost continuous film of copper which has increased in thickness. However, in comparison with the Sn-Pd sample (e), that presents a continuous coating, a few pin hole voids remain in the sample of Figure 11(d). These observations are thought to be related to the copper nanoparticle concentration. This was estimated from the Z-average recorded at the time samples were taken, using the method described in [38]. The nanoparticle concentration was calculated to be 5.89×10^{8} particles cm^{-3} (Z- Average ø 300 nm) after 1 min of processing and increased to 2.97×10^{9} particles cm^{-3} (Z- Average ø 175 nm) and 3.88×10^{9} particles cm^{-3} (Z- Average ø 160 nm) after 15 and 30 mins respectively. Therefore, longer ultrasonic processing times lead to smaller cluster sizes, a higher concentration of copper nanoparticles and therefore more catalytic sites for electroless plating to take place when the dispersion is dispensed onto a substrate. This in turn leads to more copper islands which have a greater chance to overlap and grow and form a continuous film over the substrate.

To summarise, ultrasonic dispersion of a relatively small amount of dry powder and subsequent drop coating has allowed a non-conducting substrate

to be covered in an increasing number of catalytic 'nanoislands' with a large active surface area. This surface is ideal for electroless copper activation and the deposition of a conductive copper coating. Pin holes in the copper film were observed, but with further process optimisation a copper catalyst has the potential to match the performance of a Pd based product.

4. Conclusions

This work has characterized the dispersion of a commercially available copper nanopowder using ultrasound to generate low wt. / vol. % concentration mixtures of copper nanoparticles. Low frequency ultrasound was found to be more effective than high frequency ultrasound at de-agglomerating the powder, and dispersion with a 20 kHz ultrasonic probe was very effective at breaking apart large agglomerates containing weakly bound clusters of nanoparticles. Using optimum ultrasonic processing conditions, micron agglomerates were reduced in size to sub 100 nm clusters. High intensity processing with a tapered tip did not improve the breakage rate and there appeared to be a point at which the forces generated by ultrasonic cavitation were insufficient to overcome the cohesive bonds between particles or smaller aggregates. Drop coatings of the copper dispersions were found to have excellent catalytic activity and show potential to be used in an inexpensive low wt. / vol. % catalytic ink for subsequent electroless copper plating.

Acknowledgement

The authors would like to thank the EPSRC for funding this research through the Innovative Electronics Manufacturing Research Centre (IeMRC),

Grant Number EP/H03014X/1. In addition, the authors are grateful to the industrial collaborators, Chestech Ltd, Printed Electronics Ltd and Graphic Plc for technical support and provision of materials. The authors are also grateful to the Loughborough Materials Characterisation Centre for the TEM analysis.

References

[1] C.A. Deckert, Electroless copper plating, A Review. Part I, Plating and Surface Finishing 82 (2) (1995) 48-56.

[2] X. Cui, D.A. Hutt, P.P. Conway, Evolution of microstructure and electrical conductivity of electroless copper deposits on a glass substrate, Thin Solid Films 520 (2012) 6095-6099.

[3] C.R. Shipley, US patent No. 30111920, Method of depositing a metal on a surface of a non-conducting substrate (1961).

[4] J.E. Graves, M.T. Goosey, D. Hirst, M.A. Poole, An electrochemical pre-treatment and catalysation process for ABS utilising Silver(II) chemistry, Transactions of the Institute of Metal Finishing 79 (3) (2001) 90-94.

[5] C.A. Deckert, Electroless copper plating, A Review Part II, Plating and Surface Finishing 82(3) (1995) 58-64.

[6] J.T. Kenney, US Patent No. 3783005, Method of depositing a metal on a surface of a non-conducting substrate, (1974).

[7] W.R. Brasch, EP Patent No. 0044878, A stable aqueous colloid for the activation of non-conductive substrates and the method of activating, (1982).

[8] A.J. Cobley, D.J. Comesky, L. Paniwnyk, T.J. Mason, Through hole plating of printed circuit boards using ultrasonically dispersed copper nanoparticles, Circuit World 36 (3) (2010) 9-13.

[9] Y. Wang, Y. Li, C. Rong and J. P. Liu, Sm–Co hard magnetic nanoparticles prepared by surfactant-assisted ball milling, Nanotechnology 18 (46) (2007) 465701.

[10] A.W. Pacek, P. Ding, A.T. Utomo, Effect of energy density, pH and temperature on de-aggregation in nano-particles/water suspensions in high shear mixer, Powder Technology 173 (2007) 203-210.

[11] T.J. Mason, D. Peters, Practical Sonochemistry, Power ultrasound uses and applications, (2nd Edition), Ellis Horwood Publishing, Chichester, 2002.

[12] K.S. Suslick, D.J. Casadonte, M.L.H. Green, M.E. Thompson, Effects of high intensity ultrasound on inorganic solids, Ultrasonics 25 (1987) 56-59.

[13] P. Ding, A.W. Pacek, De-agglomeration of goethite nanoparticles using ultrasonic comminution device, Powder Technology 187 (2008) 1-10.

[14] P. Ding, A.W. Pacek, Effect of pH on de-agglomeration and rheology/morphology of aqueous suspensions of goethite nanopowder, Journal of Colloid and Interface Science 325 (2008) 165-172.

[15] C. Sauter, M.A. Emin, H.P. Schuchmann, S. Tavman, Influence of hydrostatic pressure and sound amplitude on the ultrasound induced dispersion and de-agglomeration of nanoparticles, Ultrasonics Sonochemistry 15 (2008) 517-523.

[16] G. Petzold, R. Rojas-Reyna, M. Mende, S. Schwarz, Application relevant characterization of aqueous silica nanodispersions, Journal of Dispersion and Science Technology 30 (2009) 1216-1222.

[17] R. Mondragon, J. Enrique Julia, A. Barba, J.C. Jarque, Characterization of silica-water nanofluids dispersed with an ultrasound probe: A study of their physical properties and stability, Powder Technology 224 (2012) 138-146.

[18] K.A. Kusters, S.E. Pratsinis, S.G. Thoma, D.M. Smith, Ultrasonic fragmentation of agglomerate powders, Chemical Engineering Science, 48 (24) (1993) 4119-4127.

[19] K.A. Kusters, S.E. Pratsinis, S.G. Thoma, D.M. Smith, Energy-size reduction laws for ultrasonic fragmentation, Powder Technology, 80 (1994) 253-263.

[20] P. Ding and A.W. Pacek, Ultrasonic processing of suspensions of haematite nanopowder stabilised with polyacrylate, Particle Technology and Fluidization 55(11) (2009) 2796-2806.

[21] S. Markovic, M. Mitric, G. Starcevic, D. Uskokovic, Ultrasonic de-agglomeration of barium titanate powder, Ultrasonics Sonochemistry 15, (2008) 16-20.

[22] J.P.Guillemin, E. Schaer, P. Marchal, C. Lemaitre, H. Nonnet, A. Ledieu, A mass conservative approach to model the ultrasonic de-agglomeration of ZnO nanoparticle suspension in water, Powder Technology 219 (2012) 59-64.

[23] Y. Hwang, J.Lee, J. Lee, Y. Jeong, S. Cheong, Y.Ahn, S.H. Kim, Production and dispersion stability of nanoparticles in nanofluids, Powder Technology 186 (2008) 145-153.

[24] V.S. Nguyen, D. Rouxel, R. Hadji, B. Vincent, Y. Fort, Effect of ultrasonication and dispersion stability on the cluster size of alumina nanoparticles in aqueous solutions, Ultrasonics Sonochemistry 18 (2011) 382-388.

[25] V.S. Nguyen, D. Rouxel, B. Vincent, Dispersion of nanoparticles: From organic solvents to polymer solutions, Ultrasonics Sonochemistry 21 (2014) 149-153.

[26] A.N. Ivanov, Ultrasonic dispersion of Al-AlN and Al_2O_3 nanopowder agglomerates and of nanostructured AlOOH particles, Russian Physics Journal, 54(12) (2012) 1413-1416.

[27] A. Sesis, M. Hodnett, G. Memoli, A.J. Wain, I. Jurewicz, A.B. Dalton, J.D. Carey, G. Hinds, Influence of acoustic cavitation on the controlled ultrasonic dispersion of carbon nanotubes, Journal of Physical Chemistry B, 117, (48) (2013) 15141-15150.

[28] Y.A. Hernandez, V.A. Nicolosi, M.A. Lotya, F.M. Blighe, Z. Sun, S. De, I.T. McGovern, B. Holland, M. Byrne, Y.K. Gun'ko, J.J. Boland, P. Niraj, G. Duesberg, S. Krishnamurthy, R. Goodhue, J. Hutchison, V. Scardaci, A.C. Ferrari, J.N. Coleman, High-yield production of graphene by liquid-phase exfoliation of graphite, Nature Nanotechnology 3 (2008) 563-568.

[29] S. Notley, Highly concentrated aqueous suspensions of graphene through ultrasonic exfoliation with continuous surfactant addition, Langmuir 28 (2012) 14110-14113.

[30] K.S. Suslick, D.J. Casadonte, S.J. Doktycz, The effects of ultrasound on nickel and copper powders, Solid State Ionics 32-33(1) (1989) 444-452.

[31] K.S. Suslick, D.J. Casadonte, S.J. Doktycz, Ultrasonic irradiation of copper powder, Chemistry of Materials 1(1) (1989) 6-8.

[32] M. Grouchko, A. Kamyshny, K. Ben-Ami, S. Magdassi, Synthesis of copper nanoparticles catalysed by pre-formed silver nanoparticles, J. Nanopart. Res. 11 (2009) 713-716.

[33] T.J. Mason, J.P. Lorimer, Applied Sonochemistry, Wiley-VCH, Weinheim, 2002.

[34] W. Lauterborn, C. Ohl, Cavitation bubble dynamics, Ultrasonics Sonochemistry, 4 (2) (1997) 65–75.

[35] Y. Wang, P. Chen, M. Liu, Synthesis of well-defined copper nanocubes by a one pot solution process, Nanotechnology 17 (2006) 6000-6006.

[36] I. Lisiecki, F. Billoudet, M.P. Pileni, Control of the Shape and Size of Copper Metallic Particles, J. Phys. Chem 100 (1996) 4160-4166.

[37] G.H. Chan, J. Zhao, E. Hicks, G.C. Schatz, R.P.V. Duyne, Plasmonic properties of copper nanoparticles fabricated by nanosphere lithography, Nanotechnology Letters 7(7) (2007) 1947-1952.

[38] D.J. Lewis, T.M. Day, J.V. MacPherson, Z. Pikramenou, Luminescent nanobeads: Attachment of surface reactive Eu(III) complexes to gold nanoparticles, Chemical Communications 13 (2006) 1433-1435.

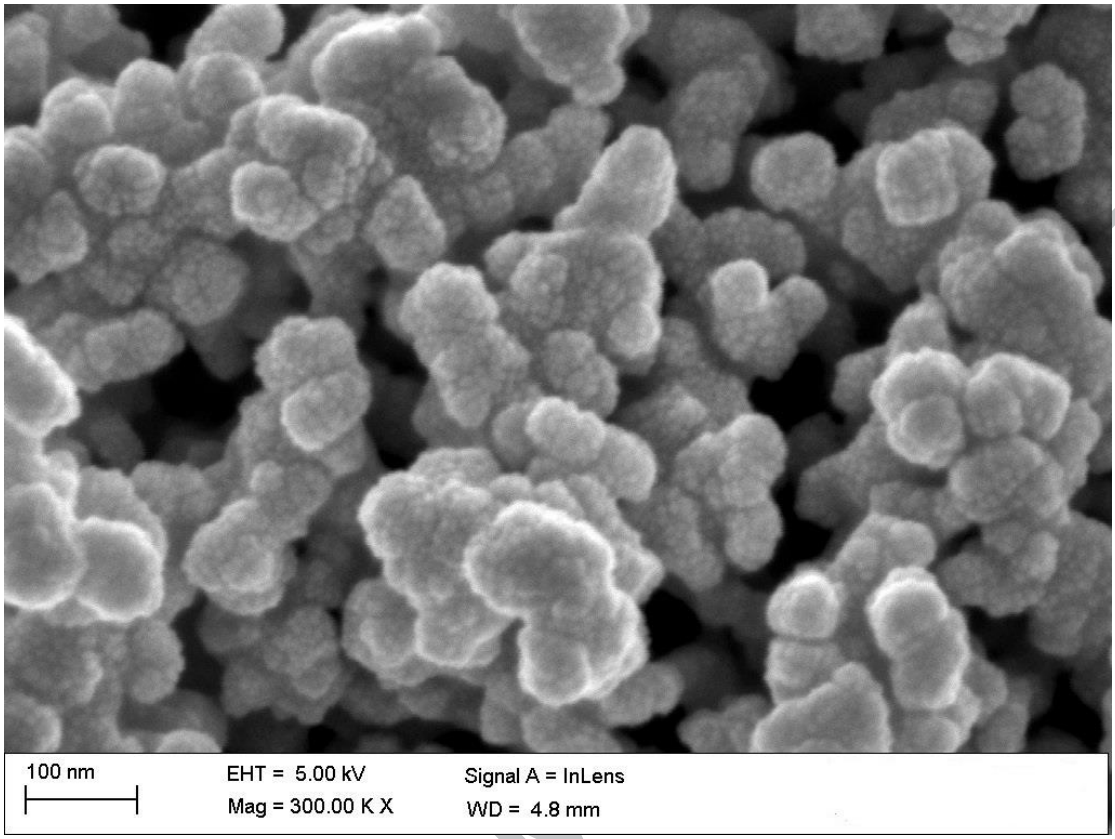

Figure 1. Scanning electron micrograph of as received copper nanoparticles.

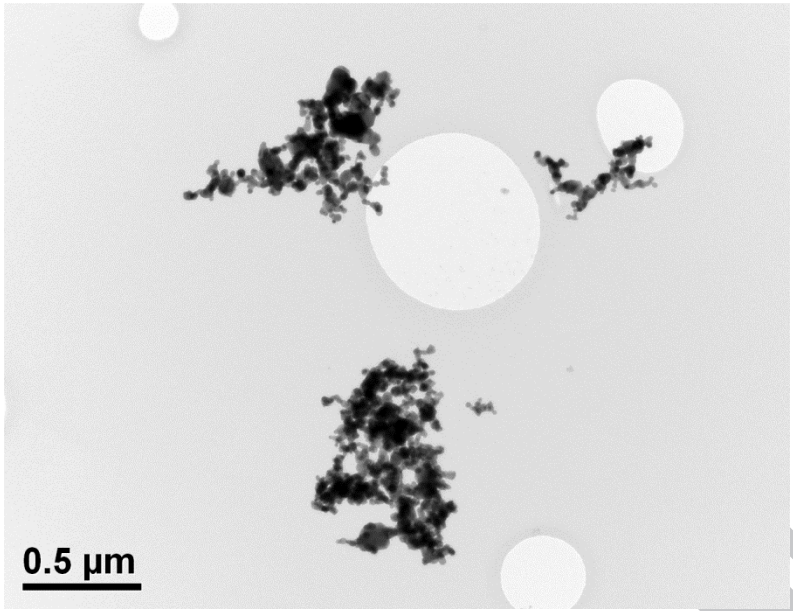

(a)

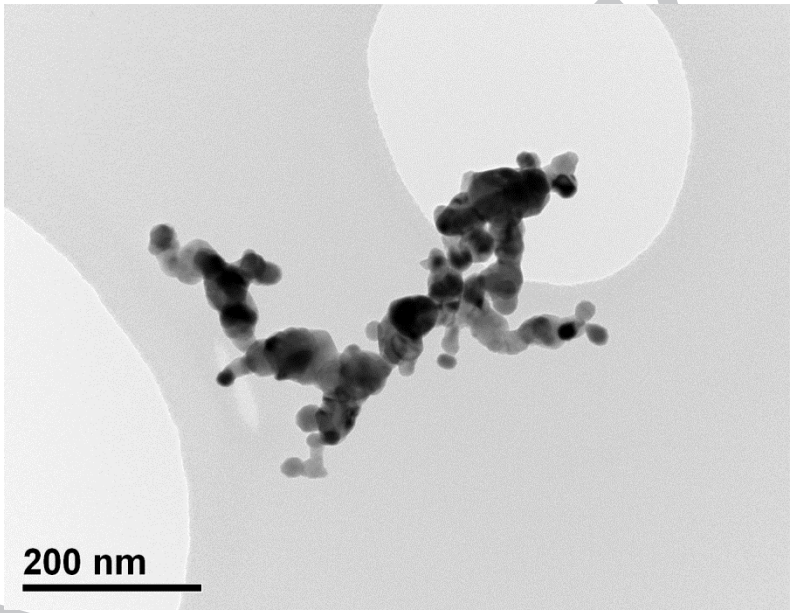

(b)

Figure 2. Transmission electron micrographs of as received copper nanoparticles dispersed in propan-2-ol with a short 10 s burst of ultrasound, 20 kHz, 100% amplitude (a) image of nanoparticle clusters and (b) higher magnification image of one of the nanoparticle clusters.

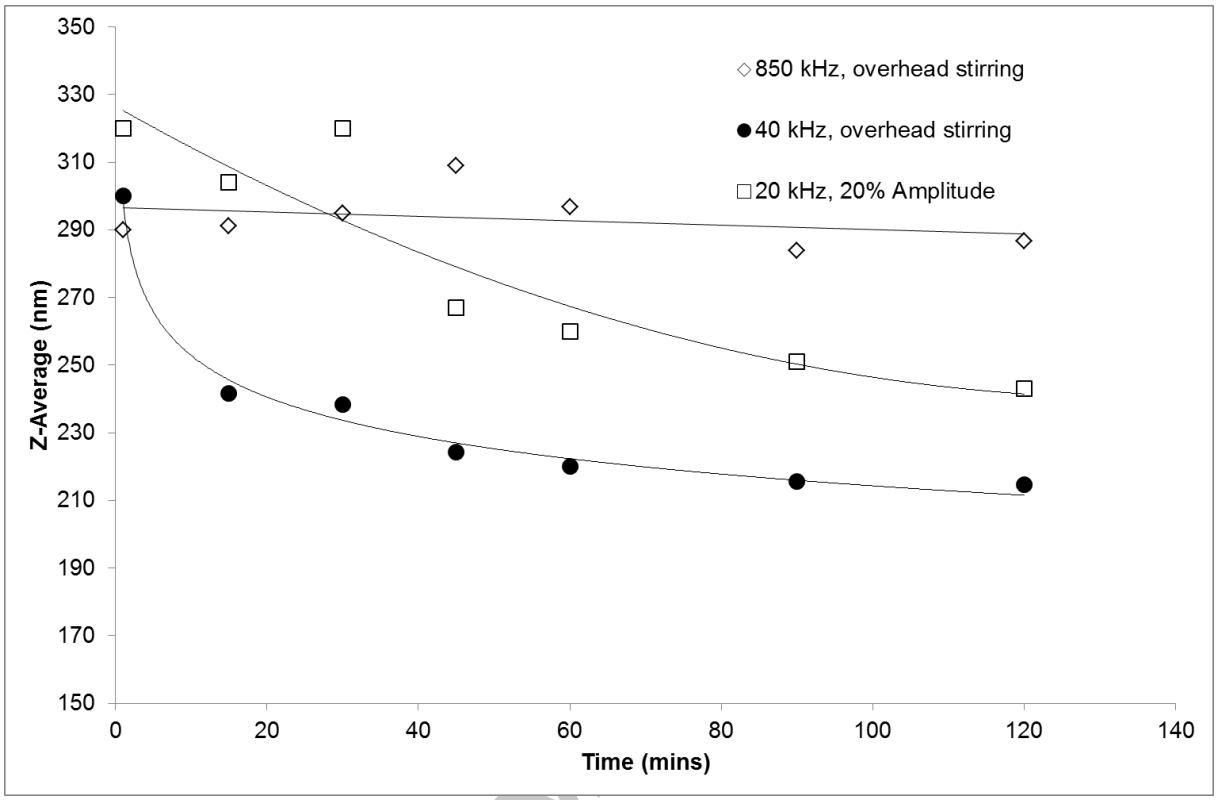

Figure 3. Evolution of mean copper nanoparticle cluster size versus ultrasonic processing time for three different ultrasonic operating frequencies operating at a constant power of 0.13 W cm^{-3}.

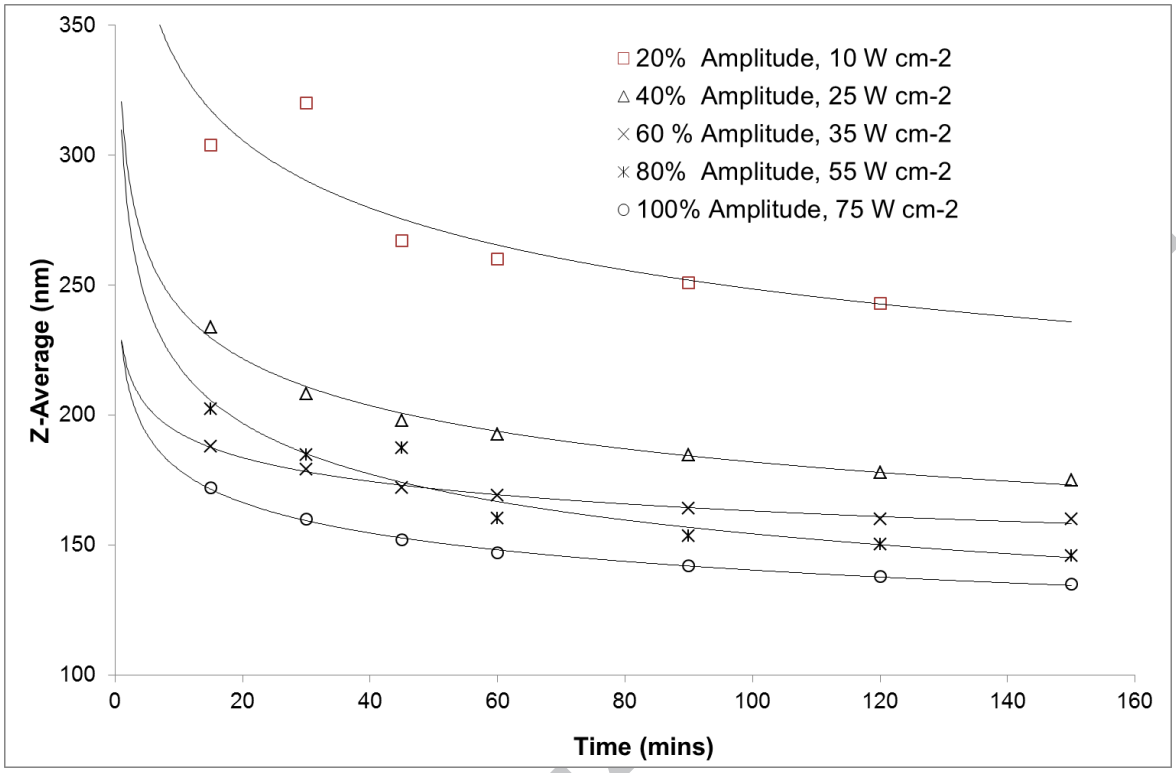

(a)

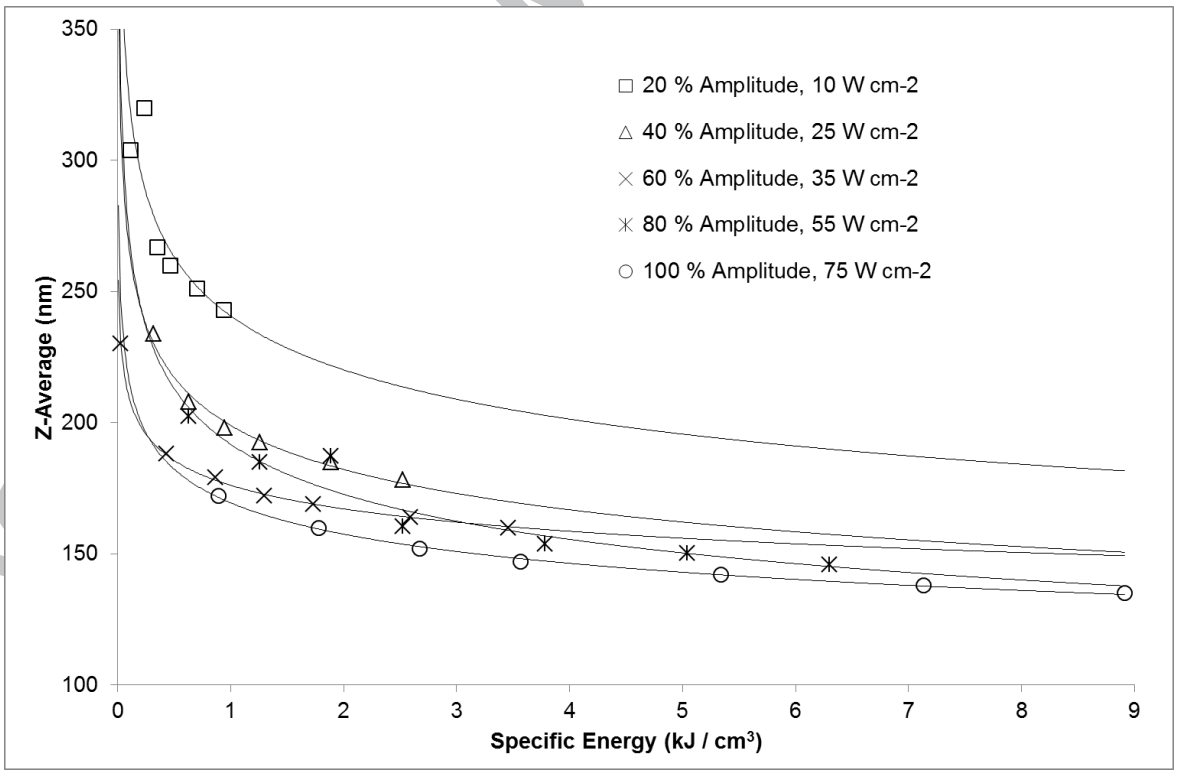

(b)

Figure 4. Evolution of mean copper nanoparticle cluster size using a 20 kHz ultrasonic probe, 1.3 cm diameter replaceable tip, for different operating intensities (a) as a function of ultrasonic processing time (b) as a function of specific energy input.

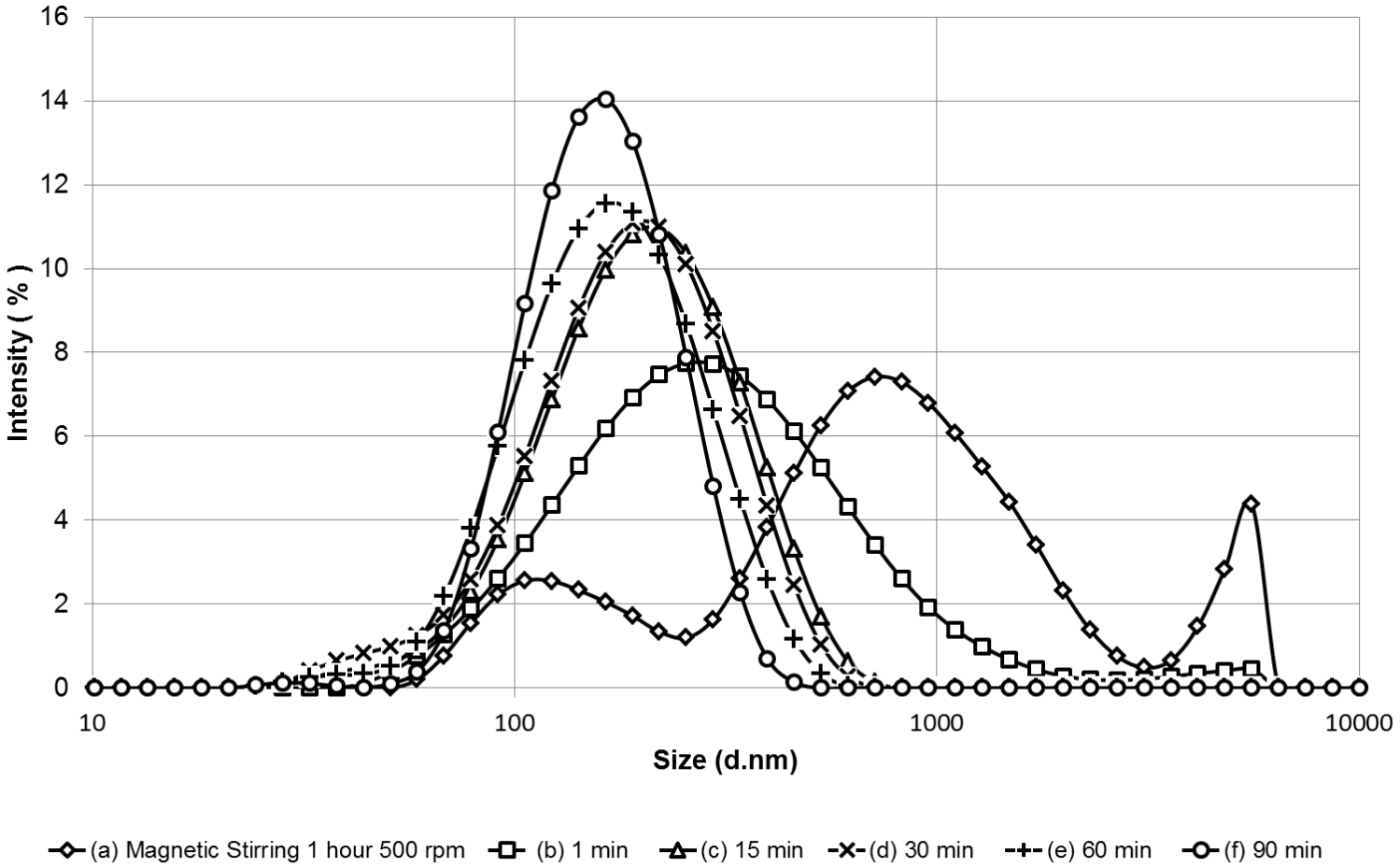

Figure 5. Copper nanoparticle cluster size distribution - intensity plots after 20 kHz ultrasonic probe, 1.3 cm diameter replaceable tip, 100 % amplitude compared with magnetic stirring.

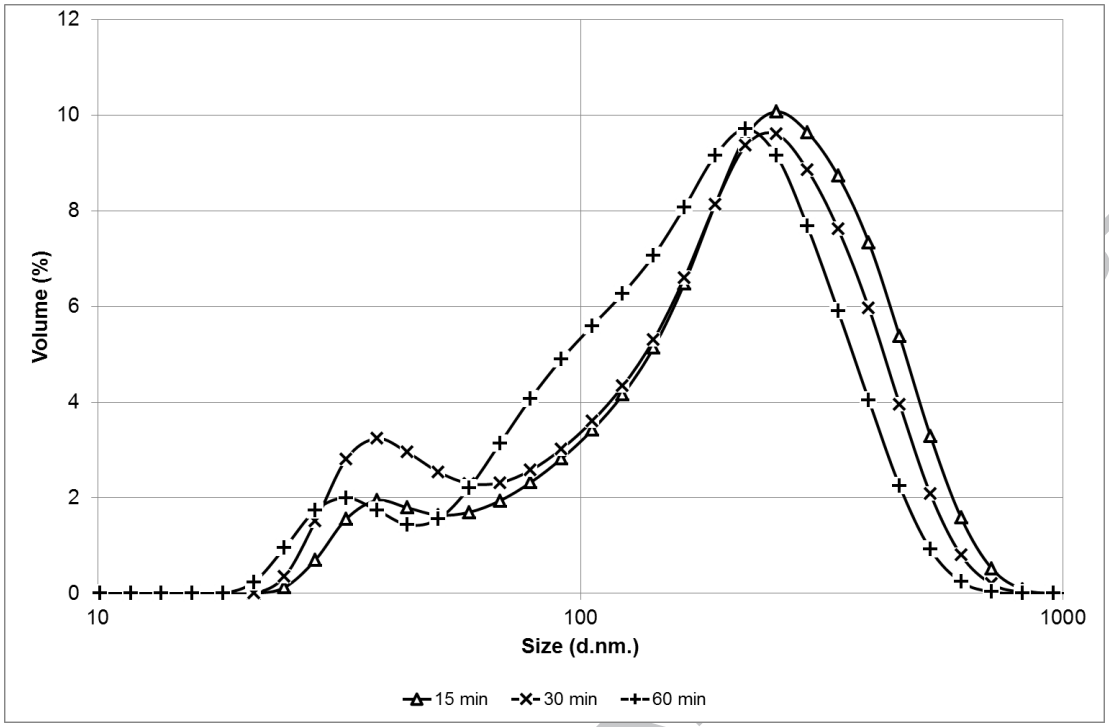

(a)

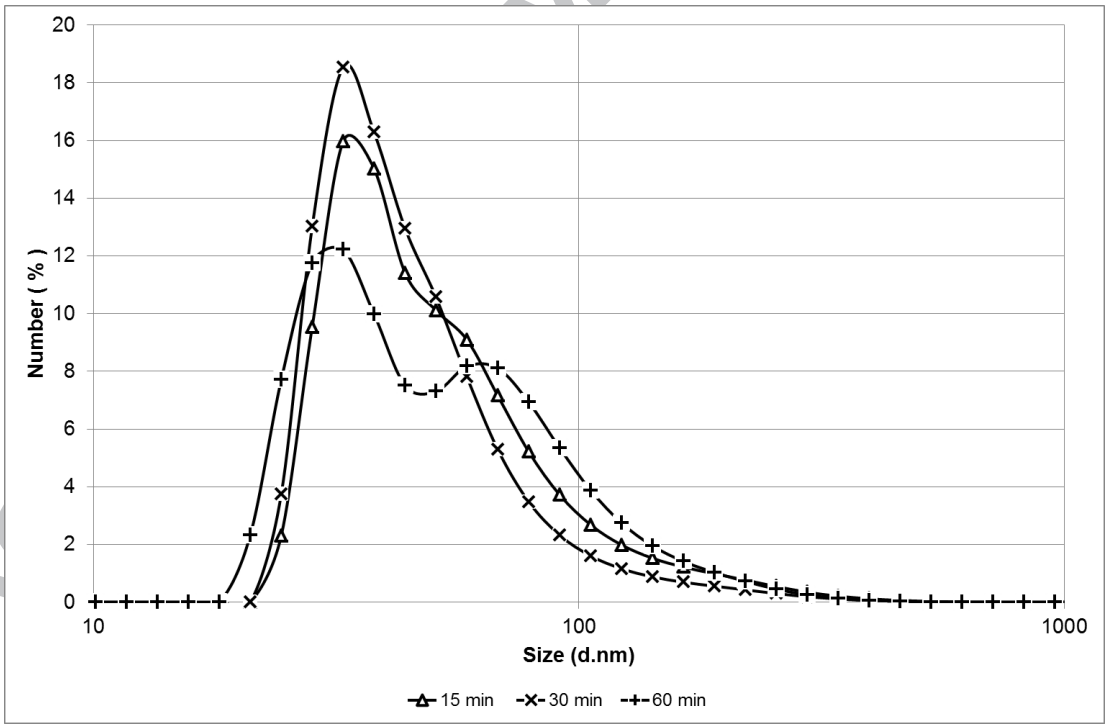

(b)

Figure 6. Copper nanoparticle cluster size distributions after processing with a 20 kHz ultrasonic probe, 1.3 cm diameter replaceable tip, 100% amplitude (a) volume plot and (b) number plot.

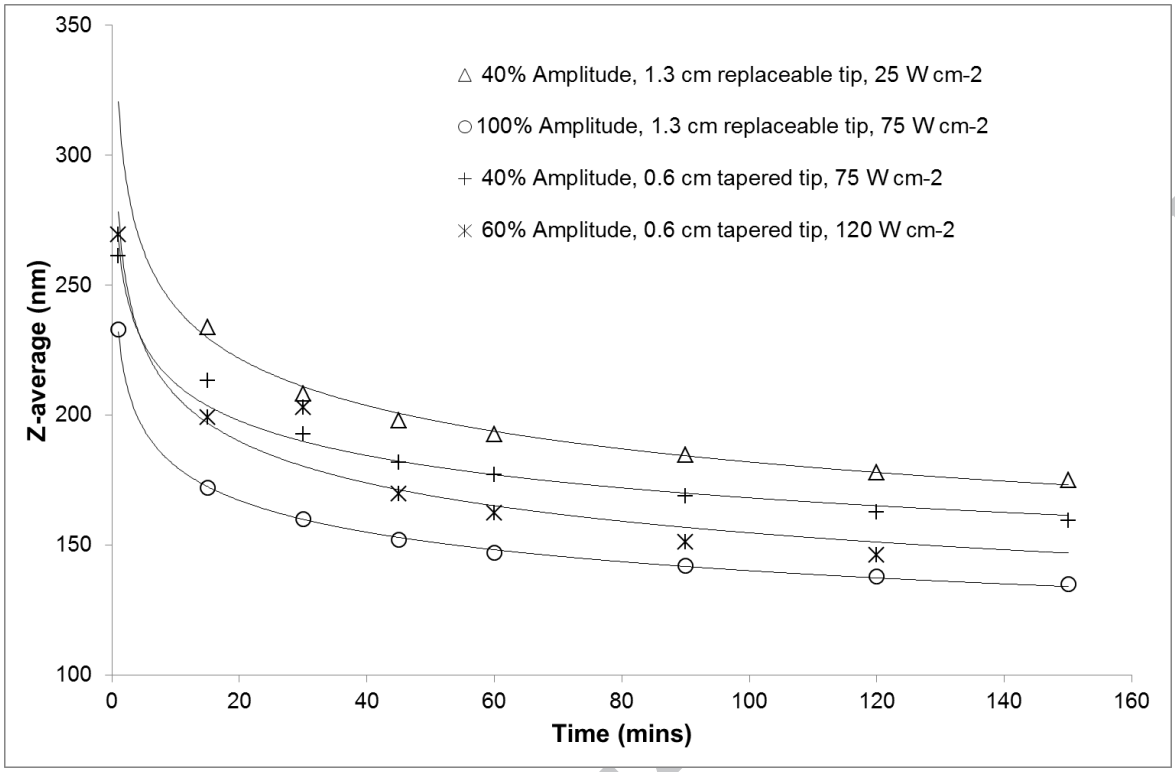

(a)

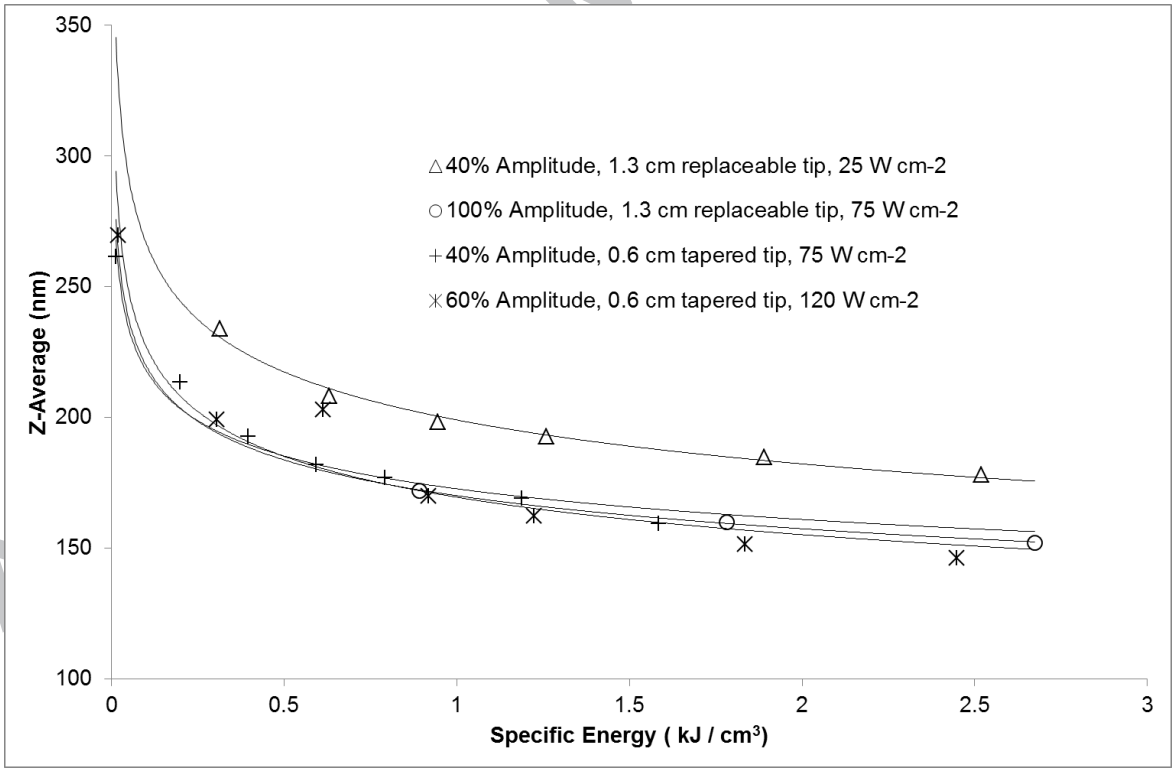

(b)

Figure 7. Evolution of mean copper nanoparticle cluster size using a 20 kHz ultrasonic probe, 1.3 cm diameter replaceable tip or a 0.6 cm diameter tapered tip, for different operating intensities (a) as a function of ultrasonic processing time (b) as a function of specific energy input.

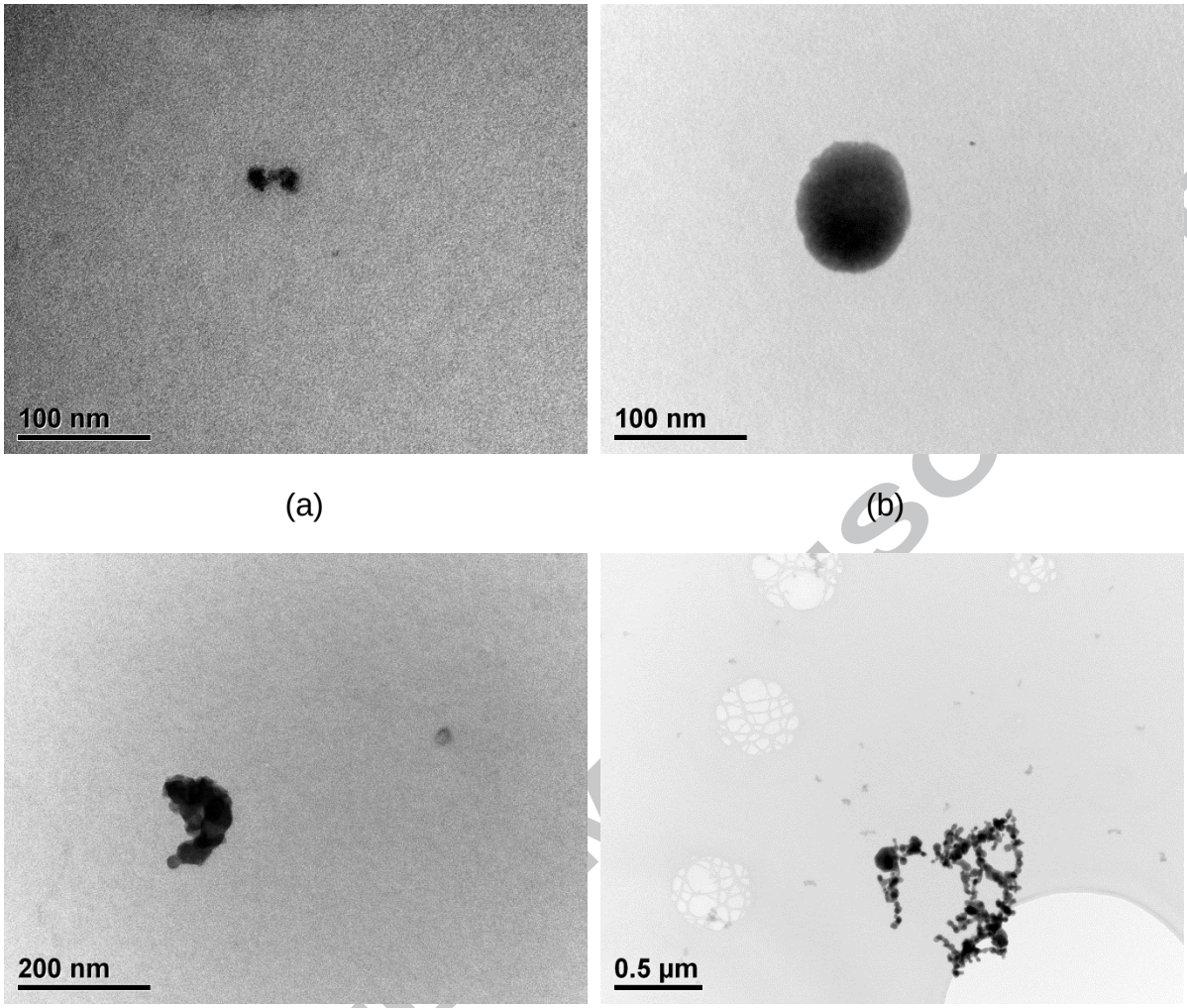

Figure 8. TEM micrographs of copper aggregates after ultrasonic dispersion in propan-2-ol using a 20 kHz ultrasonic probe, 100 % amplitude, 30 min processing time, (a) sub 50 nm (b) sub 100 nm and (c) 25nm and sub 200nm aggregate side by side (d) low magnification image of large aggregates in the foreground and sub 100nm aggregates in the background.

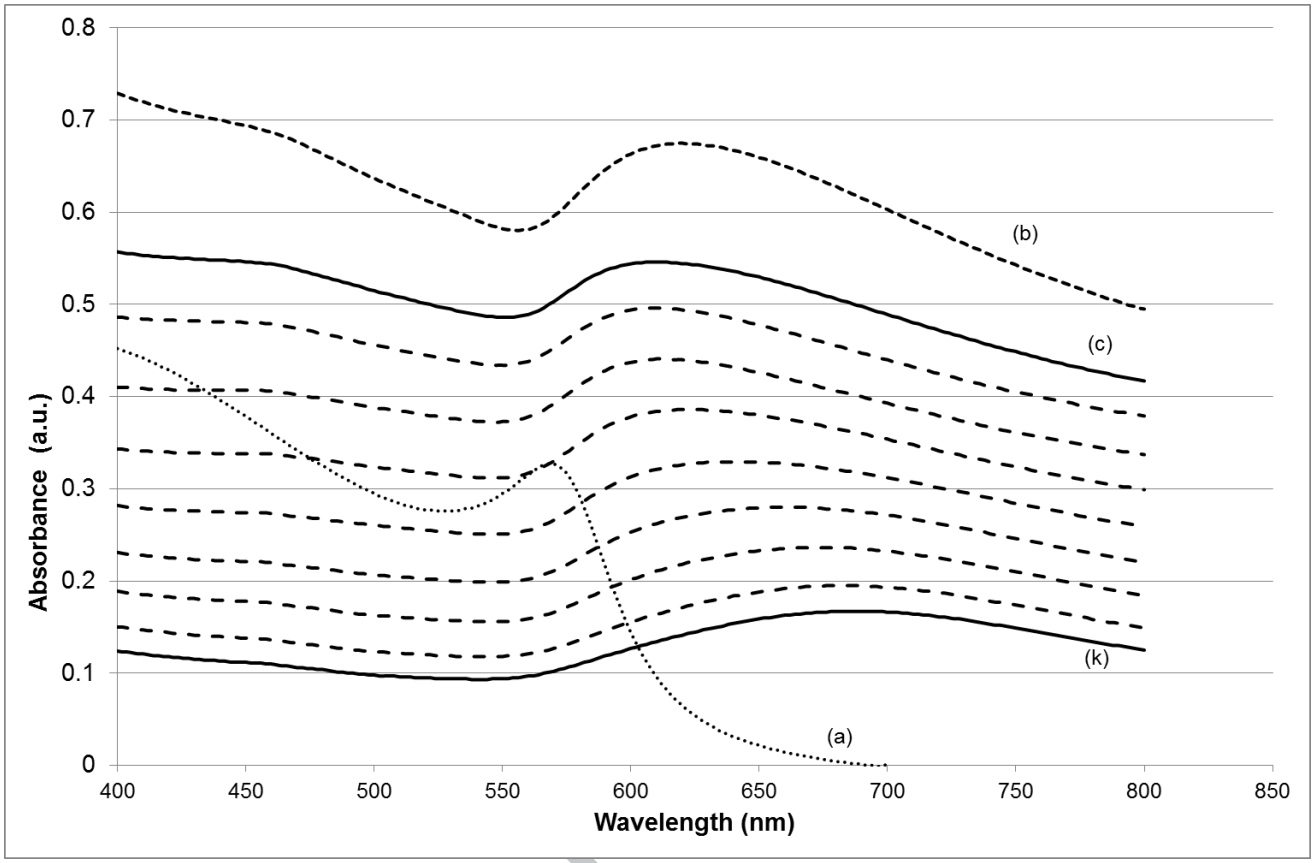

Figure 9. Absorption spectra of dispersions of Cu nanoparticles (a) chemically synthesised (0.1 ml dispersion diluted in 3 ml water), (b) copper nanopowder dispersed with 20 kHz ultrasound, (c) – (k) monitored every 3 min after the addition of glacial acetic acid. The upper and the lower solid spectra were monitored 1min and 25 min after the addition of glacial acetic acid, respectively.

(a) (b)

Figure 10. Photograph of copper nanopowder in propan-2-ol before (a) and after 30 mins of 20 kHz ultrasonic processing (b).

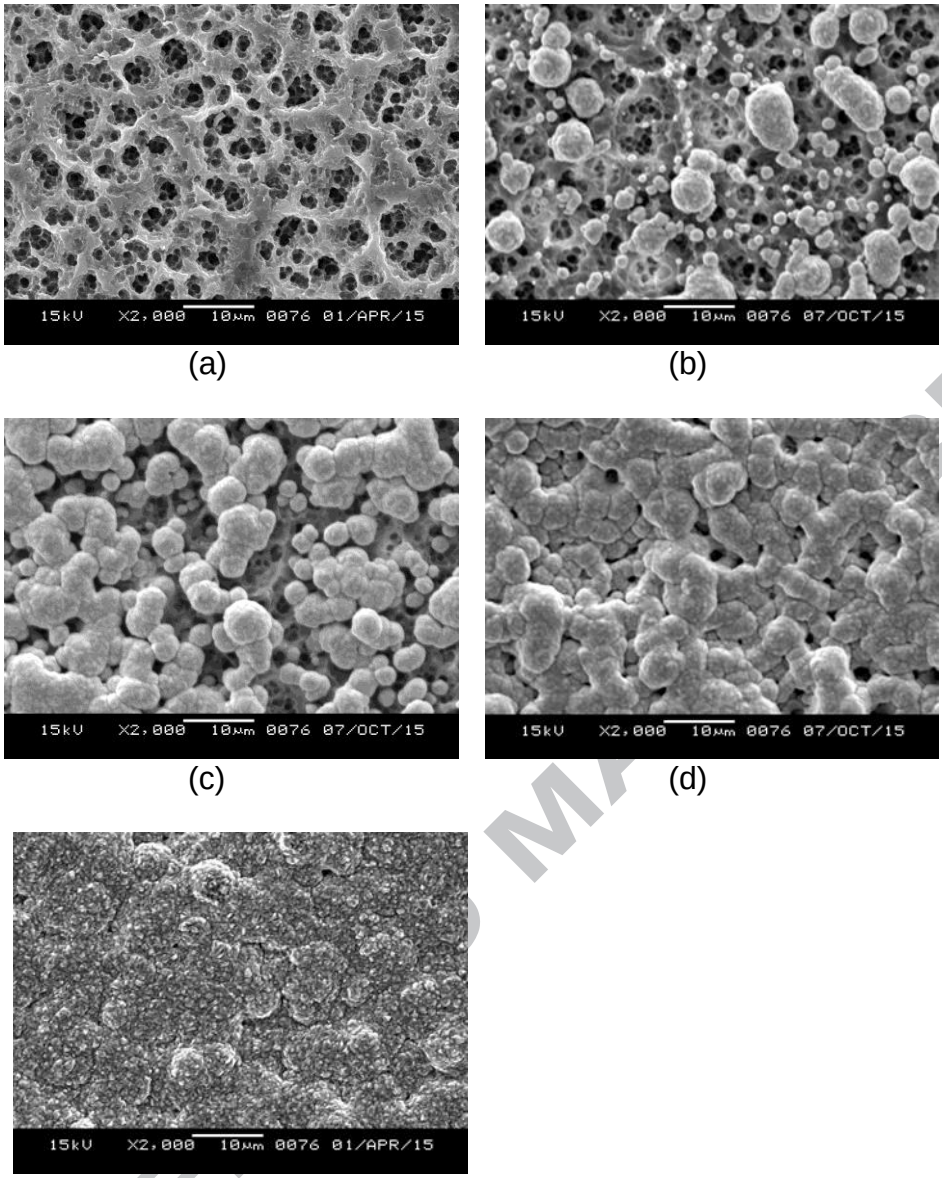

Figure 11. SEM micrographs of FR-4 substrate as received (a) and after electroless plating for 25 mins after activation by drop coating with 0.5 cm^3 of Cu NP dispersion (0.01g Cu NP in 100 cm^3 propan-2-ol) that had been dispersed with 1 min of 20 kHz ultrasonic processing (b) 15 min of 20 kHz ultrasonic processing (b) 30 min of 20 kHz ultrasonic processing (c). For comparison FR-4 substrate dip coated with a Sn / Pd colloid and plated with electroless Cu for 25 mins is shown in (e).

Table 1. Percentage reduction in Z-average between 15 - 45 min and 90 – 120 min for different amplitudes, 20 kHz ultrasonic probe, 1.3 cm diameter replaceable tip.

Amplitude/%	*Time / min*			*Time/ min*		
	15	45		90	120	
	Z-average / nm		*Reduction in Z-average / %*	*Z-average / nm*		*Reduction in Z-average / %*
20	305	265	13	250	240	4
40	235	200	15	185	180	3
60	190	170	11	165	160	3
80	200	185	8	155	150	3
100	170	150	12	140	140	0

- Expensive palladium based catalysts are typically used to metallize non-conducting substrates.
- Low concentration mixtures of a dry, agglomerated copper nanopowder were dispersed in propan-2-ol using high and low frequency ultrasound.
- DLS, TEM and absorption spectroscopy were used to characterize the dispersions.
- Low frequency ultrasound was found to be very effective at de-agglomerating the powder and breaking apart large agglomerates into sub 100 nm clusters.
- Drop coatings of the copper dispersions were found to have excellent catalytic activity and have potential to be used in an inexpensive low wt. / vol. % catalytic ink for subsequent electroless copper plating.